Experimental and numerical study of the gap resonances in-between two rectangular barges

Bernard Molin, Fabien Remy, A. Camhi, A. Ledoux

Experimental and numerical study of the gap resonances in-between two rectangular barges

B. MOLIN, F. REMY
École Centrale de Marseille & IRPHE, 13 451 Marseille cedex 20, France

A. CAMHI, A. LEDOUX
Principia, ZI Athélia 1, 13 705 La Ciotat cedex, France

ABSTRACT

Model tests are carried out with two side by side rectangular barge models rigidly linked to the carriage. Free surface elevations are measured at 9 locations along the gap. The experiments are run for two gap widths and two bilge shapes (square and rounded). RAOs of the free surface elevations derived from tests in irregular waves are compared with numerical RAOs from a linear potential flow software. In the sharp bilge case the calculated values overpredict the measurements. Numerical calculations are then performed with the gap covered by a row of massless plates, each plate being assigned a quadratic damping force with respect to its vertical velocity. With a proper choice of the drag coefficient, good agreement is obtained with the experimental RAOs.

1. INTRODUCTION

With the development of gas consumption, there has been increasing examples of side by side operations. This is the case, for instance, of LNG offloading from a LNG-carrier onto a FSRU (Floating Storage Regaseification Unit) or a GBS (Gravity Base Structure). A phenomenon that takes place in such situations is large resonant vertical motion of the free surface in the gap in-between the two hulls. It has been noticed that linear sea-keeping softwares over-predict the Response Amplitude Operators (RAOs) of the free surface elevations in the gap. As a result the low-frequency second-order loads acting on either hull are poorly predicted, which is quite damageable for the design of the fenders, hawsers and loading arms.

To remedy this problem, Huijsmans *et al.* (2001) have proposed to apply a "lid technique", that is the free surface in the gap is replaced by a solid plate. This is effective to suppress unrealistic values of the second-order forces but, obviously, does not reflect the physics correctly. Chen (2004) has proposed to introduce a linear dissipation term in the free surface equation. Newman (2003) models the free surface motion in the gap through the generalized mode technique, each mode being affected a damping term, also linear. Fournier *et al.* (2006) use both methods, as incorporated within HYDROSTAR and WAMIT, with comparable results. However Pauw *et al.* (2007), in the case of a 4 m gap, comment that no unique value of the "epsilon" coefficient (the damping term in the free surface equation) can lead to an overall good agreement between experiments and computations (see also Bunnik *et al.* 2009).

In this paper we first report on an experimental campaign that took place in the offshore wave-tank BGO-First. Two identical rectangular barges were rigidly attached to the carriage and submitted to irregular sea-states. The bilges were successively square and rounded. Experimental RAOs derived from the measured wave elevations along the gap are compared with computed ones, with Principia's software DIODORE. In the computations the gap is covered with a row of 15 plates, and each plate is assigned, not a linear, but a quadratic damping force.

2. EXPERIMENTAL CAMPAIGN

The experiments took place in the offshore wave-tank BGO-First located in la Seyne-sur-mer, near Toulon. This tank is 40 m long and 16 m wide. The waterdepth was set at 3 m during the tests.

Two identical rectangular barges were rigidly linked

to the carriage, as shown in figure 1. As a result their wave responses were restrained. The barge models had a length of 2.47 m, a width of 0.60 m and a draft of 0.18 m. The bilges were successively square then rounded, with a radius of curvature equal to 4 cm. Two gap widths were modeled: 12 and 31 cm.

Figure 1: Barge models in the tank.

The instrumentation consisted in 9 resistive wave gauges on the centerline of the gap, every 30 cm: as a result wave gauge 1 was set slightly inside the gap, at 3.5 cm from the bows of the barges, wave gauge 5 was at mid-ship and wave gauge 9 at 3.5 cm from the aft.

The barge system was submitted to irregular sea-states with Pierson-Moskowitz spectra of peak periods 1 s and 1.5 s. At the lower peak period of 1 s, the significant wave-heights were 2, 4 and 6 cm. At the higher one (1.5 s), they were equal to 3 and 6 cm. Four headings were considered: 0, 30, 60 and 90 degrees.

3. ESTIMATES OF RESONANT FREQUENCIES

Gap resonances have much similarity with moonpool resonances. As in Molin (2001), resonant modes and their frequencies can be estimated on the assumptions of infinite waterdepth, infinite beams of the motionless barges, and with the Neumann condition ($\partial\varphi/\partial x \equiv 0$) at the moonpool ends replaced with a Dirichlet condition ($\varphi \equiv 0$). The natural frequencies are then obtained as (Molin *et al.* 2002):

$$\omega_n^2 \simeq g\,\lambda_n\,\frac{1+J_n\,\tanh\lambda_n\,h}{J_n+\tanh\lambda_n\,h} \qquad (1)$$

where

$$J_n(r) = \frac{2}{n\,\pi^2\,r}\left\{\int_0^1 \frac{r^2}{u^2\,\sqrt{u^2+r^2}}\left[1+2u +(u-1)\,\cos(n\,\pi\,u)-\frac{3}{n\,\pi}\,\sin(n\,\pi\,u)\right]\,du \right.$$
$$\left. -\frac{1}{\sin\theta_0}+1+2r\,\ln\frac{1+\cos\theta_0}{1-\cos\theta_0}\right\} \qquad (2)$$

with $\lambda_n = n\,\pi/l$, $r = b/l$ and $\tan\theta_0 = r^{-1}$. Here l is the length of the gap, b its width and h its draft.

This calculation leads to the following values of the first six natural frequencies ω_n (in rad/s):

Table 1: Estimated resonant frequencies for the two gap widths of 12 cm and 31 cm.

Mode	1	2	3	4	5	6
12 cm	5.53	6.21	6.86	7.52	8.17	8.82
31 cm	4.65	5.61	6.46	7.25	8.00	8.71

Odd number modes are symmetric with respect to midship, while even number modes are antisymmetric.

4. LINEAR CALCULATIONS

We focus on the narrower gap case (12 cm), for which resonances are more pronounced.

Computations were performed with the software DIODORE of Principia. Figure 2 presents the mesh used for the computations. The number of panels is 4990 per barge. Since the free surface RAOs in the gap exhibit many sharp peaks, calculations were done every 0.01 s for wave periods in the range [0.7 s 1.5 s].

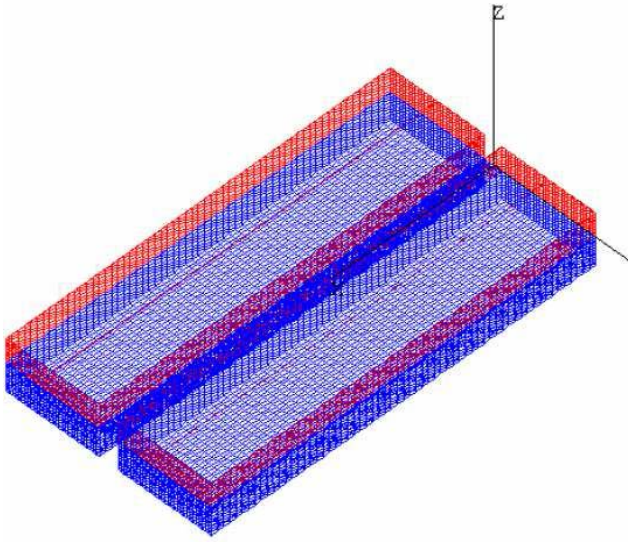

Figure 2: Mesh for DIODORE calculations.

We assumed first that whether the bilges were modeled as square or rounded would lead to the same free surface RAOs. As a matter of fact there are slight

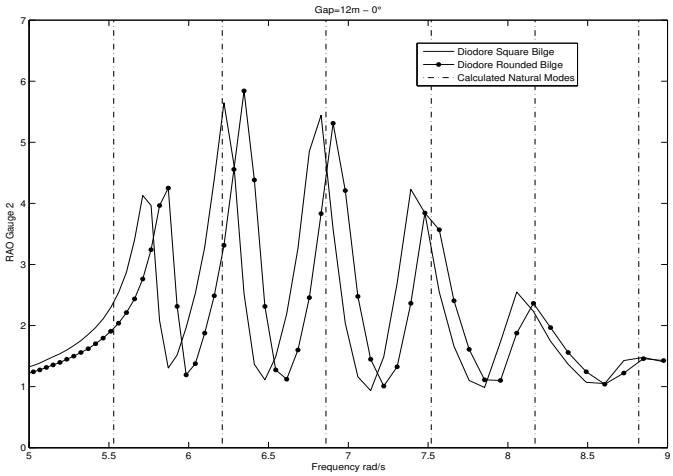

Figure 3: RAO at gauge 2, 0° heading, narrow gap. Square vs. rounded bilges.

differences. Figure 3 presents the computed RAO of the free surface elevation at gauge 2, at 0° heading, for the two bilges. In the figure are also shown the approximated resonant frequencies as obtained from equations (1) (2) and reported in Table 1: the first resonant frequency is underestimated but the others are quite close to the predictions. Note that RAO values up to 6 are attained at the peaks.

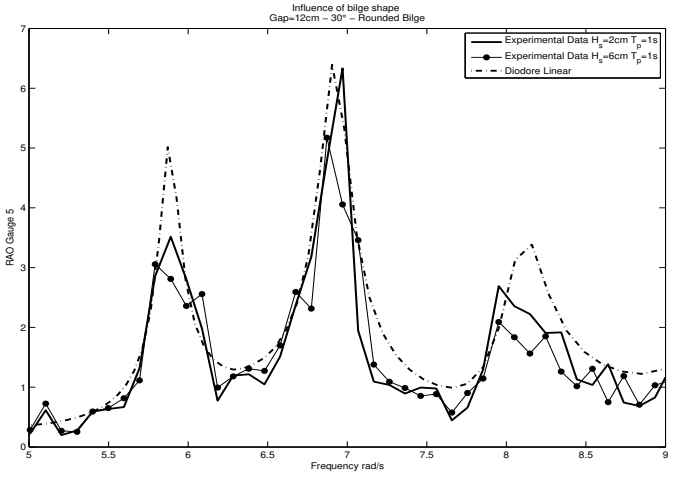

Figure 4: Rounded bilges. Heading 30°. Numerical and experimental free surface RAOs at gauge 5.

Figures 4 and 5 show RAOs of the free surface elevation at wave gauge 5, in the 30 degrees heading case (narrow gap), as calculated with DIODORE and as derived from the experiments in the two seastates $[H_S = 2$ cm, $T_P = 1$ s$]$ and $[H_S = 6$ cm, $T_P = 1$ s$]$. Figure 4 is for the rounded bilges case, figure 5 for

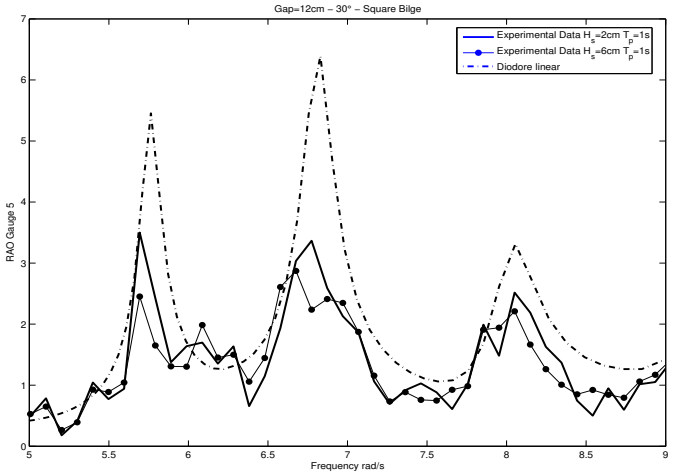

Figure 5: Square bilges. Heading 30°. Numerical and experimental free surface RAOs at gauge 5.

the square bilges case. It can be observed that, in the rounded bilges case, the experimental and numerical RAOs agree rather well, albeit the experimental ones are slightly lower, whereas in the square case the experimental RAOs are much lower than the numerical ones. This suggests that the decrease of the RAOs is mostly due to flow separation at the bilges. In this respect the RAO reduction has much analogy with the roll damping of barges near resonance. For sharp bilges the viscous roll damping moment is usually represented as quadratic with respect to the roll velocity (Ledoux *et al.* 2004).

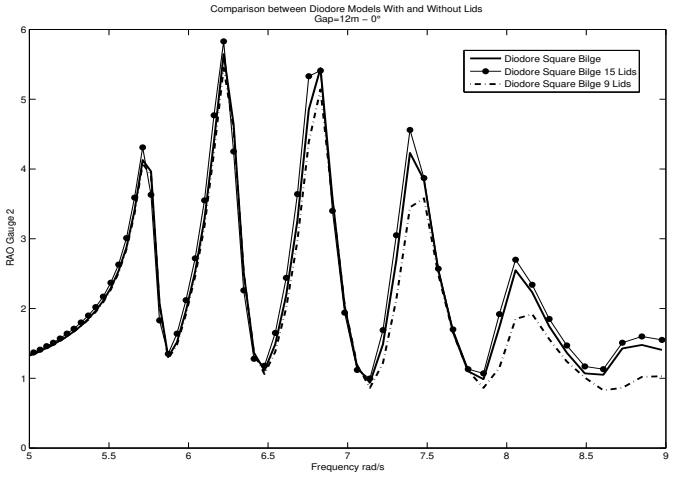

Figure 6: RAO at gauge 2, 0° heading, square bilges. Calculated values with and without plates at the free surface.

The methodology that has been devised within DIODORE to tackle this problem is to cover the gap with a succession of massless plates, and to assign to

each of them a quadratic damping force with respect to its vertical velocity. The open question is which value to assign to the drag coefficient. Some relevant information has been available from previous investigations on moonpool problems (see Molin *et al.* 2002).

The gap was first covered with 9 plates, each plate having 3 degrees of freedom in heave, roll and pitch, and being discretized with 49 panels. Nine plates turned out to be too coarse at high frequencies and the number of plates was increased to 15.

Figure 6 presents the obtained free surface RAOs, at gauge 2 at 0° heading (alike in figure 3), according to the initial calculations (no plate), and with the 9 and 15 plates, with no viscous damping being assigned. It can be seen that the initial and 15 plates results are in very good agreement over the considered frequency range.

5. COMPARISONS BETWEEN EXPERIMENTS AND CALCULATIONS

As written above the tests were run in irregular waves only. The produced seastates lasted 10 minutes in the basin, meaning about 1000 wave cycles at the 1 s peak period and 700 cycles at the 1.5 s peak period. Measured elevations were processed through cross spectral analysis to yield the experimental RAOs. In this process one must be aware that it is difficult to extract precise RAOs with a small frequency spacing.

5.1 Narrow gap, square bilges

Based on previous experience (Molin *et al.* 2002), a drag coefficient equal to 0.5 was selected. In the DIODORE calculations, so-called stochastic linearization is being applied, delivering RAOs that are seastate dependent.

Figures 7 and 8 relate to the 30° heading and present numerical and experimental RAOs obtained at wave gauge 2 for the two seastates [$H_S = 2$ cm, $T_P = 1$ s] (figure 7) and [$H_S = 6$ cm, $T_P = 1$ s] (figure 8). In both figures the RAO initially computed, without viscous damping, is also given. The decrease of the experimental RAOs, as the severity of the seastates increases, is evident. Also noticeable is a small shift toward lower frequencies, presumably associated with third-order free surface non-linearities. With the selected drag coefficient of 0.5, the numerical RAOs are in fair agreement with the experimental ones.

Figures 9 through 16 relate to the 90° heading (beam waves). The free surface motion in the gap is then

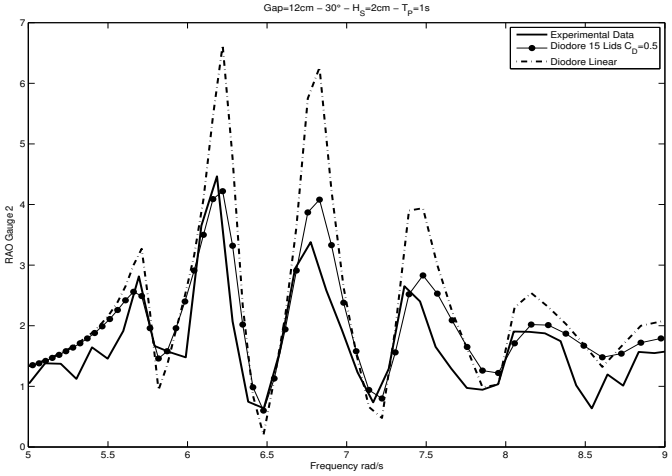

Figure 7: Heading 30°. $H_S = 2$ cm, $T_P = 1$ s. Free surface RAO at gauge 2.

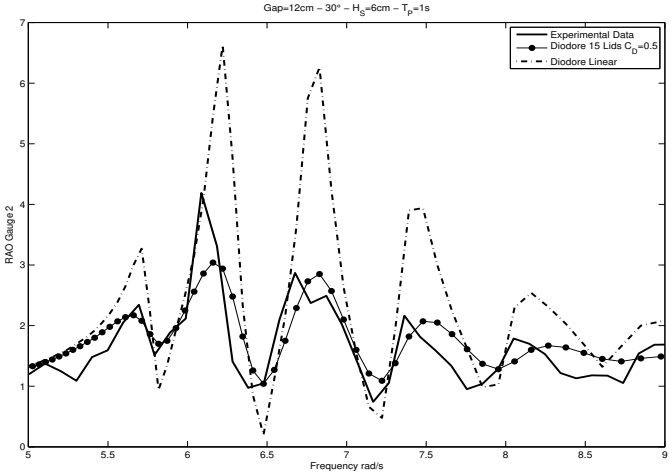

Figure 8: Heading 30°. $H_S = 6$ cm, $T_P = 1$ s. Free surface RAO at gauge 2.

symmetric with respect to midship. As a result only symmetric modes (with numbers 1, 3, 5 and 7 in Table 1) appear. Experimental and numerical RAOs, for the two seastates of peak period 1 s and significant waveheights 2 and 6 cm, are shown at gauge 2 (figures 9 and 10), 3 (figures 11 and 12), 4 (figures 13 and 14), and 5 (figures 15 and 16). The overall agreement is rather good. The sensitivity of the experimental RAOs to the severity of the seastate appears to be well rendered by the quadratic damping term.

5.2 Wide gap

Finally we give a few results in the case of the 31 cm gap. Figures 17 and 18 show the calculated and measured RAOs of the free surface elevations at gauge 5, in

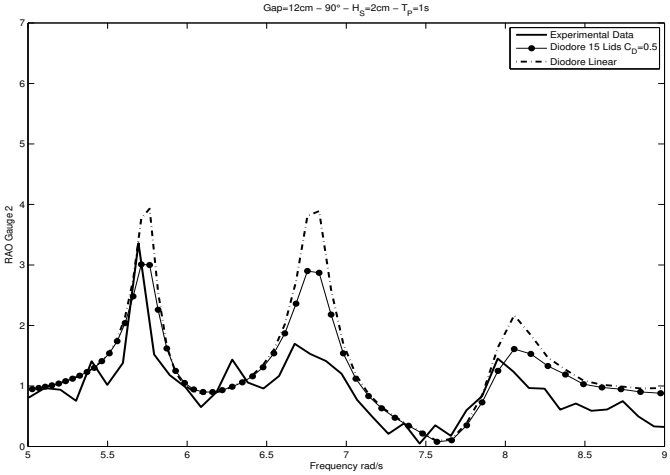

Figure 9: Heading 90°. $H_S = 2$ cm, $T_P = 1$ s. Free surface RAO at gauge 2.

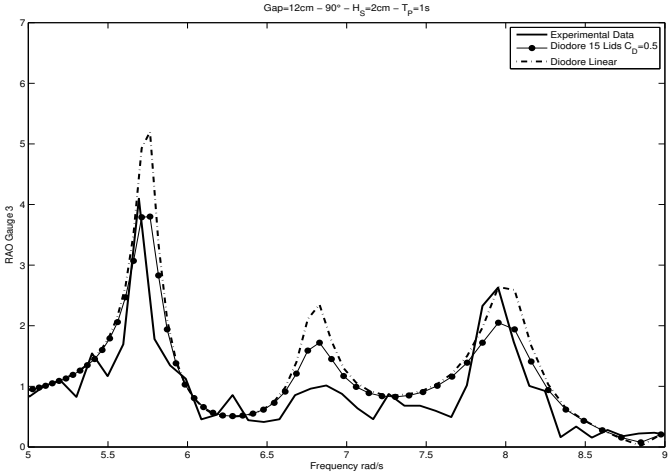

Figure 11: Heading 90°. $H_S = 2$ cm, $T_P = 1$ s. Free surface RAO at gauge 3.

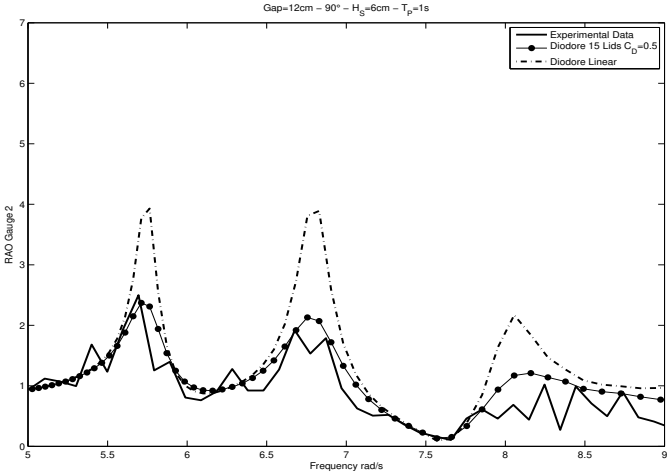

Figure 10: Heading 90°. $H_S = 6$ cm, $T_P = 1$ s. Free surface RAO at gauge 2.

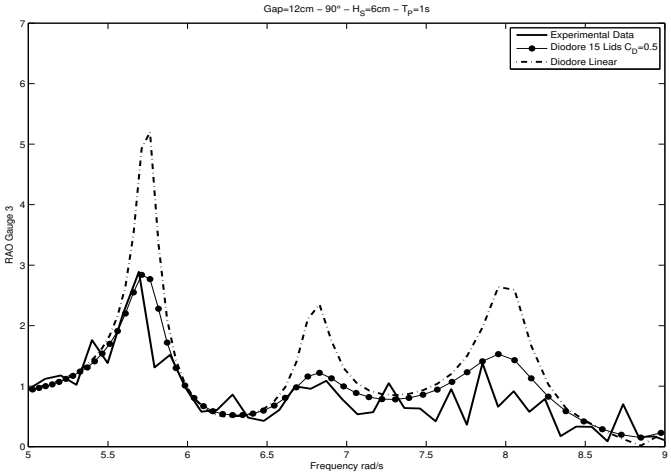

Figure 12: Heading 90°. $H_S = 6$ cm, $T_P = 1$ s. Free surface RAO at gauge 3.

the square (figure 17) and rounded (figure 18) cases. The numerical peaks are much lower and much less pronounced than in the narrow gap case. Therefore linear calculations do a rather good job and it does not appear necessary to introduce further damping terms.

5.3 Drift forces

In this section we present some results obtained for the drift forces. The hydrodynamic loads on the models were not measured during the experiments so these results are purely numerical. All the results that follow refer to the small gap width (12 cm), with the sharp bilges.

The drift forces are calculated through Lagally's theorem (Ledoux *et al.* 2006). This formulation permits to discriminate between the two bodies with a better numerical accuracy than the pressure integration (or *near-field*) method.

Figure 19 shows the calculated wave drift force in sway, normalized by $\rho\, g\, l\, A^2$ (l being the length of the barges and A the wave amplitude), acting on either hull, in head waves. The computations are done without additional damping, with and without the gap being covered by the 15 plates. The sway drift force is repulsive on either hull, and attains very large values.

Figure 20 gives the sway drift force at the same heading, with the viscous damping force being applied to the vertical motion of the plates. The results are given for the two seastates [$H_S = 2$ cm, $T_P = 1$ s] and [$H_S = 6$ cm, $T_P = 1$ s], with the drag coefficient equal to 0.5. As expected the computed wave drift force is

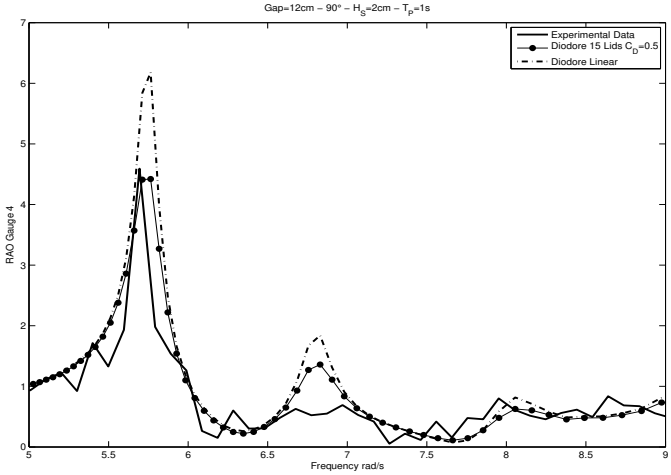

Figure 13: Heading 90°. $H_S = 2$ cm, $T_P = 1$ s. Free surface RAO at gauge 4.

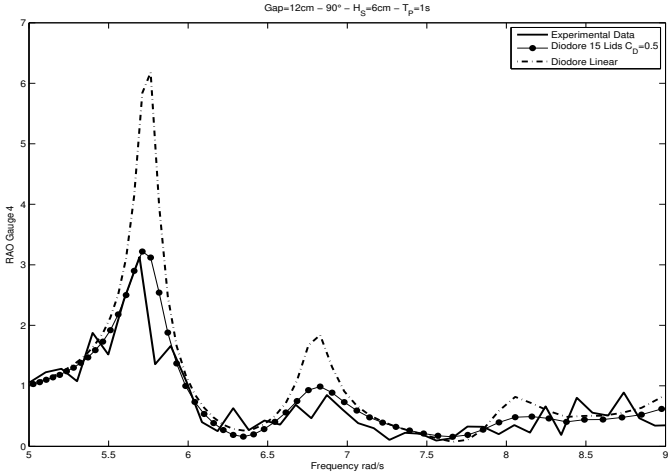

Figure 14: Heading 90°. $H_S = 6$ cm, $T_P = 1$ s. Free surface RAO at gauge 4.

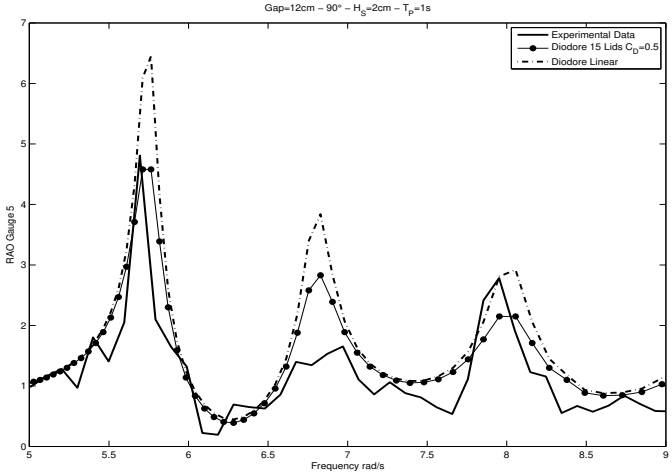

Figure 15: Heading 90°. $H_S = 2$ cm, $T_P = 1$ s. Free surface RAO at gauge 5.

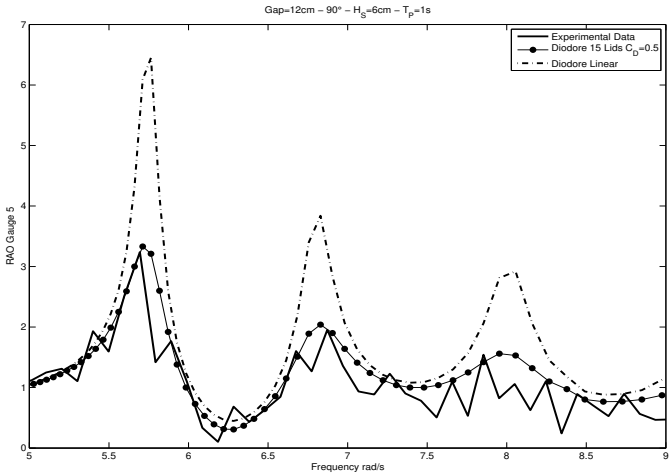

Figure 16: Heading 90°. $H_S = 6$ cm, $T_P = 1$ s. Free surface RAO at gauge 5.

highly sensitive to the seastate.

Finally we present the sway drift force in beam waves. Figure 21 shows the calculated drift force acting on the lee barge, figure 22 the calculated drift force on the upwave barge. It can be checked visually that in the high frequency range the sum of the two drift forces is close to its asymptotic value of $1/2\,\rho\,g\,l\,A^2$

6. CONCLUDING REMARKS

We have produced experimental evidence that the discrepancies between measured and calculated free surface elevations in the gap in-between two side-by-side rectangular barges are mostly due to flow separation at the bilges. This damping effect has much similarity with the viscous roll damping of FPSOs or barges at resonance.

To render this effect numerically we have covered the gap by a row of 15 massless plates, each plate being assigned a damping force quadratic with respect to its vertical velocity. In the case of the 12 cm gap, a drag coefficient equal to 0.5 has produced numerical RAOs of the free surface elevation in good agreement with the measured ones. It must be noted that these RAOs are seastate dependent, as a result of the non-linearity of the damping term. In the general case, the drag coefficient will be dependent on the aspect ratio (width over draft) of the gap. The generalization of the proposed approach to the case of freely floating ships with different drafts and/or bilge shapes also deserves further investigation.

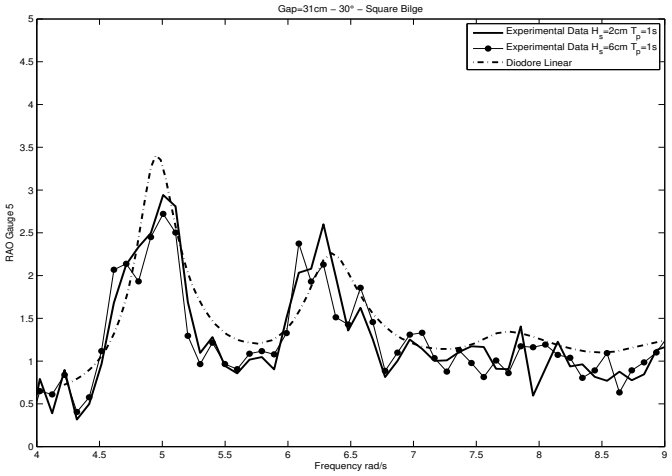

Figure 17: Large gap. Square bilges. Heading 30°. Free surface RAO at gauge 5.

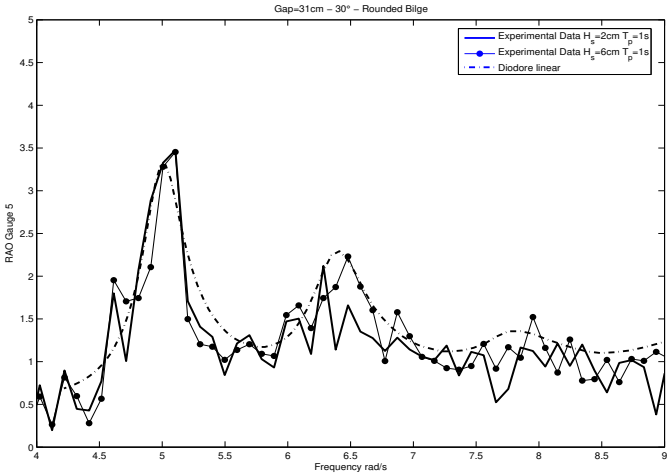

Figure 18: Large gap. Rounded bilges. Heading 30°. Free surface RAO at gauge 5.

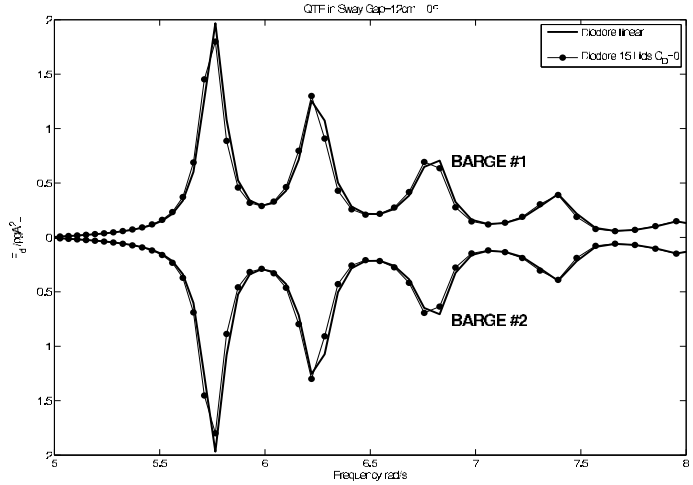

Figure 19: Calculated wave drift force in sway. Heading 0°. No viscous damping.

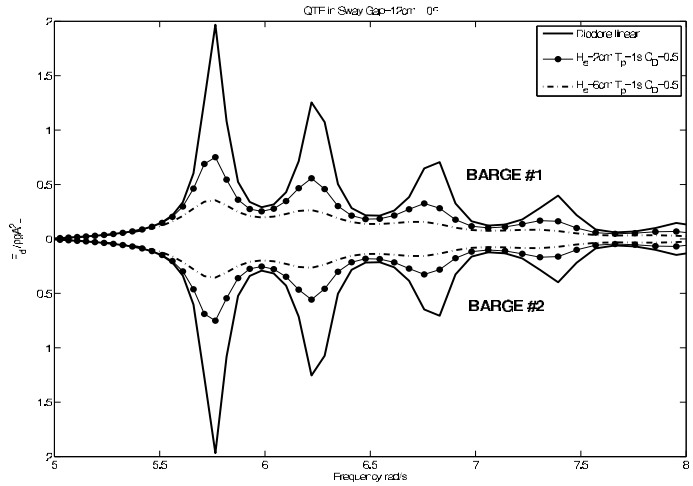

Figure 20: Calculated wave drift force in sway. Heading 0°. With viscous damping.

ACKNOWLEDGMENTS

The experiments were carried out within the GIS-HYDRO association with financial support from Conseil Général du Var.

REFERENCES

Bunnik T., Pauw W. & Voogt A. 2009 Hydrodynamic analysis for side-by-side offloading, *Proc. 19th ISOPE Conf.*, Osaka.

Chen X.-B. 2004 Hydrodynamics in offshore and naval applications - Part 1, *Proc. 6th Int. Conf. Hydrodynamics ICHD*, Perth.

Fournier J.-R., Naciri M. & Chen X.-B. 2006 Hydrodynamics of two side-by-side vessels. Experiments and numerical simulations, *Proc. 16th ISOPE Conf.*, San Francisco.

Huijsmans R.H.M., Pinkster J.A. & de Wilde J.J. 2001 Diffraction and radiation of waves around side by side moored vessels, *Proc. 11th ISOPE Conf.*, Stavanger.

Ledoux A., Molin B., Delhommeau G. & Remy F. 2006 A Lagally formulation of the wave drift force, *Proc. 21st Int. Workshop on Water Waves & Floating Bodies*, Loughborough.

Ledoux A., Molin B., de Jouette C. & Coudray T. 2004 FPSO Roll damping prediction from CFD and 2D model test investigations, *Proc. 14th ISOPE Conf.*, Toulon.

Molin B. 2001 On the piston and sloshing modes in moonpools, *J. Fluid. Mech.*, **430**, 27–50.

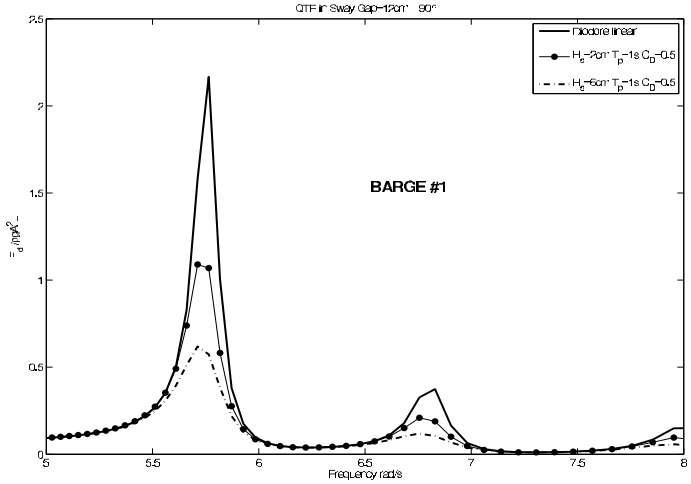

Figure 21: Calculated wave drift force in sway on the lee barge. Heading 90°. With viscous damping.

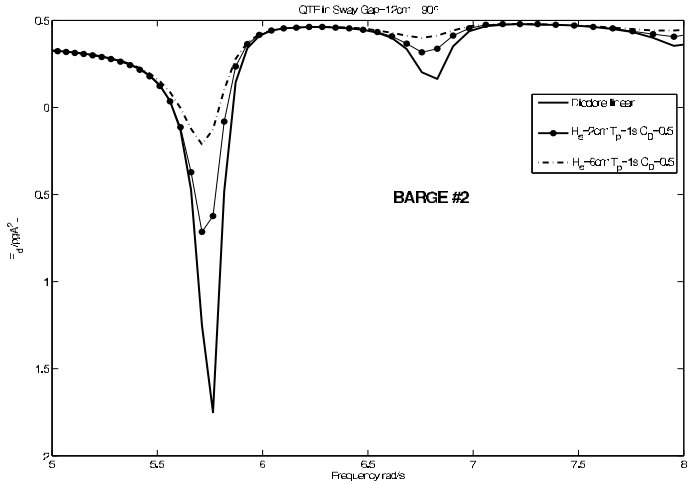

Figure 22: Calculated wave drift force in sway on the up-wave barge. Heading 90°. With viscous damping.

Molin B., Remy F., Kimmoun O. & Stassen Y. 2002 Experimental study of the wave propagation and decay in a channel through a rigid ice-sheet, *Applied Ocean Res.*, **24**, 247–260.

Newman J.N. 2003 Application of generalized modes for the simulation of free surface patches in multiple body interactions, *WAMIT Consortium Report.*

Pauw W.H., Huijsmans R.H.M. & Voogt A. 2007 Advances in the hydrodynamics of side-by-side moored vessels, *Proc. 26th OMAE Conf.*, San Diego.